Flow Turning and Admittance Correction: An Experimental Comparison

F. Vuillot* and P. Kuentzmann†
Office National d'Etudes et de Recherches Aérospatiales, Châtillon, France

The proper way of incorporating viscosity-related acoustic losses into solid propellant rocket motor linear stability analyses has been an open question for years. Mainly, two distinct theories are proposed in the literature and are referred to as the flow turning and admittance correction approaches. The two theories are briefly presented, then competitively used to derive composite solid propellant pressure-coupled response functions from experiments. The experimental setup is succinctly described and experimental results are presented. Comparisons between the theoretical approaches are made on the basis that the proper approach should yield equal values for the propellant response function, irrespective of particular grain geometry, provided that the same mean chamber pressure and frequency are achieved in the chamber. Results favor the admittance correction approach, as the flow turning approach seems to overestimate viscous losses.

Nomenclature

a = speed of sound
A = dimensionless admittance, $=\rho_o a_o v'/p'$
Cp = specific heat at constant pressure
e = gas internal specific energy
eb = web distance burned
E_N^2 = acoustic energy in the chamber, $=\int_v \hat{p}_N^2 dv$
f = frequency
h = gas-specific enthalpy
i = complex number, $i=\sqrt{-1}$
Im = imaginary part
k = wave number
L = length
M = Mach number
$\dot{m}_c$ = burned gas mass flow rate
p = pressure
r = gas constant
R = radius
R_c = global pressure coupled response function; defined in Sec. II
Re = real part
$(R_e)_a$ = acoustic Reynolds number
S = chamber cross-sectional area
S_b = burning surface
u,v = axial and radial velocities, respectively
v_c = propellant regression rate
V = nozzle dimensionless admittance function
t = time
T = temperature
α = damping coefficient
γ = ratio of specific heats
δ = boundary-layer thickness
ϵ = acoustic pressure amplitude, $p'/\bar{p}$
λ = thermal conductivity
μ = molecular viscosity coefficient
ρ = density
ρ_p = propellant density
ϕ = normalized acoustic pressure amplitude; phase angle
ω = angular frequency

Subscripts and Superscripts

$(\,)_0$ = reference state
$(\,)_N$ = pure acoustic mode
$(\,)_{is}$ = isentropic value
$(\,)'$ = unsteady component
$\bar{(\,)}$ = steady component
$\hat{(\,)}$ = spatial component of a harmonic part $(\,)' = \hat{(\,)}e^{i\omega t}$
$(\,)_I$ = injection
$(\,)_L$ = entrance plane of the nozzle

Presented as Paper 85-1484 at the AIAA/ASME/SAE 21st Joint Propulsion Conference, Monterey, CA, July 8-10, 1985; received Oct. 8, 1985; revision received April 3, 1986.

*Research Engineer, Chemical Propulsion Division.
†Head, Chemical Propulsion Division.

I. Introduction

IT has long been recognized that visco-acoustic losses are of primary importance in the evaluation of the stability of solid propellant rocket motors. Theoretical and experimental works[1-6] have shown that the viscosity of the combustion gases can provide a significant amount of damping to the combustion chamber. According to Culick,[3,4] a fair estimate of the damping resulting from viscosity-acoustics interactions with wall injection was provided by the usual one-dimensional analyses, despite their inviscid nature. This estimate was termed "flow turning" by Culick. More than ten years ago, Culick[4] proposed extending the flow turning terms arising in one-dimensional analyses to multidimensional analyses. This was intended to provide the design engineer with a rough estimate of viscous losses with which to correct inviscid analyses. At this time, Flandro[5] obtained results different from Culick's by performing a theoretical treatment of unsteady viscous boundary layers with normal injection. His work demonstrated different boundary-layer responses depending on the orientation of the acoustic velocity with respect to the direction of the mean flow resulting from the combustion. This led to the "admittance correction" approach. The flow turning approach has been widely used, mainly for its relative simplicity although the admittance correction approach seems somewhat more rigorous. Recently, Van Moorhem[6] cast the flow serious doubt on the turning approach and asked again for incorporation of boundary-layer treatment into stability analyses. The main point of this last paper was to demonstrate that the assumptions giving rise to the flow turning terms in one-dimensional analyses were not rigorous enough to justify the incorporation of these terms into multidimensional analyses as suggested by Culick.

The present paper is aimed at showing experimental results permitting a comparison between the flow turning approach and the admittance correction approach.

To achieve this, the main assumptions that give rise to the flow turning terms are briefly recalled. Then a theoretical treatment of injected acoustic boundary layers is performed following Flandro's paper.[5] However, with respect to Ref. 5, further refinements are made: these mainly concern the order of magnitude discussion and are aimed at facilitating comparisons with flow turning. Then, two one-dimensional stability analyses are presented, the first identical to the one proposed by Culick,[3] which includes a flow turning term, and the other one purely inviscid (thus with no flow turning terms) to which the admittance correction approach is added. In the last part of the paper, the two methods are competitively used to obtain response function curves of composite propellants from experiments. The experimental apparatus used has been first described by Kuentzmann and Laverdant[7] and is currently in use at ONERA to determine pressure-coupled response functions at high frequencies. This apparatus will be briefly described, together with several recent improvements made to data recording and data processing.

II. Theoretical Analyses

The most classical approach used to assess the linear stability of solid propellant rocket motors is the acoustical balance approach,[1-4] whose most practical form has been developed by Culick.[2-4] In this theory, the inviscid equations of harmonic motions in the rocket chamber are linearized in terms of two small parameters: $\epsilon = |p'|/\bar{p}$ and $\bar{M}_I = \rho_p \bar{v}_c/(\rho_0 a_0)$. The acoustic balance theory ends up with a linear equation for the complex wave number: $k = \omega/a + i\alpha/a$. One consequence of linearization is that the combustion processes and the fluid mechanics are decoupled. Then, steady combustion reduces to a steady mass flow issuing normally from the burning surface, and unsteady combustion is represented by simple admittance or response functions. We will not discuss the linearization process nor the acoustic balance approach, which are treated in detail in the references.

The main point of interest here is the description of the interaction of the acoustic motions with the mass flow issuing from the burning propellant, especially when the viscosity of the combustion gases cannot be neglected. The main assumption behind the following analysis is that the flame thickness must remain much smaller than the other length scales of the problem, such as the length or radius of the chamber, the wave length of the acoustic pressure waves, and also the viscous boundary-layer thickness (Fig. 1).

A. Flow Turning in One-Dimensional Analyses

For a side burning propellant (Fig. 1), the one-dimensional inviscid equations for unsteady motions are as follows:
Continuity:

$$S\frac{\partial \rho}{\partial t} + \frac{\partial}{\partial x}(\rho u S) = \dot{m}_c$$

Axial momentum:

$$S\frac{\partial}{\partial t}(\rho u) + \frac{\partial}{\partial x}(\rho u^2 S) + S\frac{\partial p}{\partial x} = \dot{m}_c u_s$$

Energy:

$$S\frac{\partial}{\partial t}(\rho e) + \frac{\partial}{\partial x}(\rho u e S) + \frac{\partial}{\partial x}(upS) = \dot{m}_c h_I$$

where u_s is the axial velocity at the flame edge (Fig. 1). Classical one-dimensional stability analyses exhibit two additional damping terms that are absent from three-dimensional analyses. Careful examination of this result traces these additional terms back to the source terms of the one-dimensional axial momentum and energy equations. One additional term is linked to nonisentropic wall conditions ($T'_w \neq T'_{is}$) and will not be discussed here, except to mention that it can be conveniently handled by introducing a pressure-coupled propellant temperature response function, $R_{TP} = (T'_w/\bar{T})/(p'/\bar{p})$. Kuentzmann[7,9] found that R_{TP} simply adds up to the classical propellant response function R_{MP}, $R_{MP} = (v'_c/\bar{v}_c)/(p'/\bar{p})$, to form a global pressure-coupled response function, $R_c = R_{TP} + R_{MP}$. However, it has been demonstrated that R_{TP} stays close to its isentropic value, $(R_{TP})_{is} = (\gamma - 1)/\gamma$. The other additional term is linked to the axial momentum source term $\dot{m}_c u_s$ and is referred to as the flow turning term. u_s is a boundary condition for the one-dimensional model and plays an important role in the formula for the imaginary part of the complex wave number.[4,6,8] Culick[4] argues that u_s must be zero since the combustion gases enter the chamber with zero axial velocity and he arrives at an extra damping term that can be expressed as:

$$\alpha_{FT} = \frac{a_0}{2k_N^2 E_N^2}\int_{S_b} (\mathrm{d}\hat{p}_N/\mathrm{d}x)^2 \bar{M}_I \mathrm{d}s$$

However, if one derives one-dimensional equations from area-averaged three-dimensional inviscid equations,[6,8] one naturally find that u_s turns out to be the one-dimensional axial velocity u. Furthermore, taking $u_s = u$, instead of $u_s = 0$, exactly cancels out the flow turning term. This result was the basis of the criticism in Ref. 6 against flow turning.

According to Culick,[4] this precise result can be viewed as evidence that α_{FT} takes care of processes taking place in viscous boundary layers and thus can be considered as a fair estimate of viscous losses. The next step taken by Culick is to incorporate the flow turning term into three-dimensional analyses.[4]

Several remarks can be made at this point. First, u_s acts only through its unsteady part u'_s, since $\dot{m}_c \bar{u}_s$ is of second order in $\bar{M}_I$ and thus drops out in the linearization process. Hence, the physical phenomenon behind flow turning is unsteady or acoustic boundary layers with steady injection. Secondly, taking $u'_s = 0$ will force the injected mass flow to acquire the main flow acoustic velocity as soon as it has left the emitting surface. This implies a strong, perfectly inelastic interaction, which undoubtedly is an overestimation of the real-life interaction. In this view, α_{FT} should be an upper bound to the damping resulting from the interaction of the injected flow with perpendicular acoustic motions.

B. Acoustic Boundary Layers

Unsteady boundary-layer equations are derived from the laminar Navier-Stokes equations, assuming that the viscosity coefficient μ is small. The inviscid equations are modified only in a thin domain close to the wall, whose extension δ is of the order of an inverse square root acoustic Reynolds number,[5,10]

$$\delta \sim 1/\sqrt{(R_e)_a} = \sqrt{\mu_0 \omega/2\rho_0 a_0^2}$$

Furthermore, the mean flow is approximated by a uniform flow perpendicular to the emitting wall, which is parallel to the x axis (Fig. 2). Linearization of the equations is carried out as

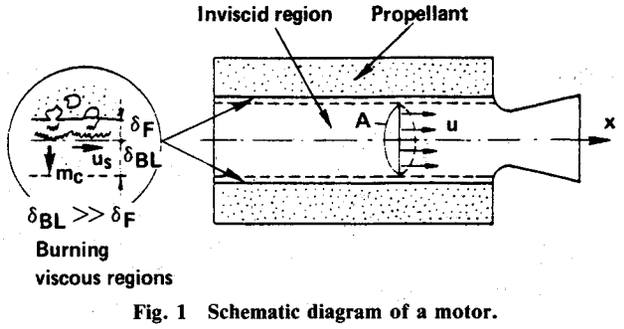

Fig. 1 Schematic diagram of a motor.

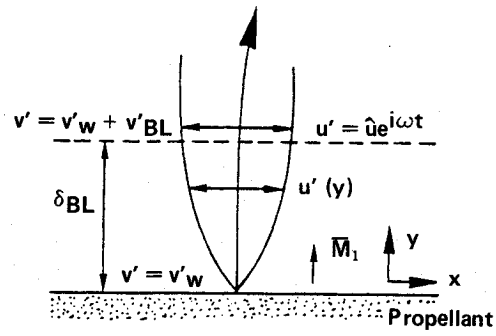

Fig. 2 Injected acoustic boundary layers.

before with the additional assumption that δ is of the order of $\bar{M}_I$. This restriction may be lifted once the proper equations are obtained, since $\bar{M}_I$ is a regular perturbation parameter.[8] The simplified unsteady equations for harmonic motions then read as follows:

$$i\omega\rho' + \rho_0\frac{\partial u'}{\partial x} + \rho_0\frac{\partial v'}{\partial y} + a_0\bar{M}_I\frac{\partial \rho'}{\partial y} = 0 \tag{1}$$

$$i\omega\rho_0 u' + \frac{\partial p'}{\partial x} - \mu_0\frac{\partial^2 u'}{\partial y^2} + \rho_0 a_0\bar{M}_I\frac{\partial u'}{\partial y} = 0 \tag{2}$$

$$\frac{\partial p'}{\partial y} = 0 \tag{3}$$

$$i\omega(c_p T' - p'/\rho_0) + c_p a_0\bar{M}_I\frac{\partial T'}{\partial y} - \frac{\lambda_0}{\rho_0}\frac{\partial^2 T'}{\partial y^2} = 0 \tag{4}$$

where

$$p' = r\rho_0 T' + rT_0\rho'$$

$$y \sim \delta \text{ and } a_0/\omega \gg \delta$$

It should be noted that no dissipation terms appear in the energy equation (4) since they are of second order in u'. Moreover, for isentropic wall conditions, Eqs. (4) and (3) yield the classical isentropic relationship $p' = a_0^2\rho'$, and Eqs. (1-4) reduce to

$$i\omega\rho' + \rho_0\frac{\partial u'}{\partial x} + \rho_0\frac{\partial v'}{\partial y} = 0 \tag{5}$$

$$i\omega\rho_0 u' + \frac{\partial p'}{\partial x} - \mu_0\frac{\partial^2 u'}{\partial y^2} + \rho_0 a_0\bar{M}_I\frac{\partial u'}{\partial y} = 0 \tag{6}$$

$$\frac{\partial p'}{\partial y} = \frac{\partial T'}{\partial y} = \frac{\partial \rho'}{\partial y} = 0 \tag{7}$$

$$p' = a_0^2\rho' \tag{8}$$

It is also worthwhile to note that finding the solution to the complete set of Eqs. (1-4) is not a major obstacle. In particular, it is possible to show that the acoustic boundary layer will damp out any nonisentropic wall conditions: indeed, it is found that R_{TP} at the boundary-layer edge is always $R_{TP} = (\gamma - 1)/\gamma$, whatever value it takes at the flame edge. Moreover, the simplified equations (5-8) show that R_{TP} need not be specified at the flame edge: this value would have been required otherwise.[5] Equations (5-8) are sufficient to permit a precise evaluation of the damping due to acoustic boundary layers to be compared to α_{FT}. Only the case of grazing acoustic waves is of interest here, and a sinusoidal pressure wave will be assumed:

$$p' = \hat{p}_0 e^{i\omega t}e^{-i(kx+\phi)}$$

Equations (5-8) are then integrated with the following boundary conditions at $y = 0$: $u' = 0$ and $v' = v'_w$. For the sake of simplicity, let $v'_w = 0$; this implies that the boundary-layer admittance derived later will be only a linear correction, to be added to the burning propellant's own admittance. Then one finds

$$\rho_0 a_0 u' = \hat{p}_0(1 - e^{-my})e^{i\omega t}e^{-i(kx+\phi)} \tag{9}$$

$$\rho_0 a_0 v' = -i\hat{p}_0(k/m)(1 - e^{-my})e^{i\omega t}e^{-i(kx+\phi)} \tag{10}$$

where

$$m = \beta(a' + ib'), \qquad a' > 0$$

with

$$\beta = \sqrt{\rho_0\omega/2\mu_0} = k\sqrt{(R_e)_a}/2$$

a' and b' are dimensionless parameters given by:

$$a'^2 - b'^2 + \bar{M}_I\sqrt{(R_e)_a}a' = 0$$

$$2a'b' + \bar{M}_I\sqrt{(R_e)_a}b' = 2$$

Simple algebra yields

$$a' = -\frac{F}{2} + \left(\frac{F^2 + \sqrt{F^4 + 64}}{8}\right)^{1/2}$$

$$b' = ((-F^2 + \sqrt{F^4 + 64})/8)^{1/2}$$

where

$$F = \bar{M}_I\sqrt{(Re)_a}$$

The acoustic boundary-layer thickness at 99% of the freestream acoustic velocity and its specific acoustic admittance are readily obtained from Eqs. (9) and (10):

$$\delta_{.99} = (4.61)/\beta a' \tag{11}$$

$$A_{BL} = \lim(\rho_0 a_0 v'/p')_{y\to\infty} = -i\omega(a' - ib')/(a_0\beta(a'^2 + b'^2)) \tag{12}$$

It should be noted that the chosen sign convention implies that a negative real part of A_{BL} corresponds to a stabilizing effect on the chamber acoustics.

Figure 3 shows the variations of $\delta_{.99}$ and of $Re(A_{BL})$ with both the frequency and the mean injection Mach number. Two remarks can be inferred from Fig. 3. First, it is found that the mass injection thickens the boundary layer to the point that in the low-frequency range and for injection Mach numbers typical of rocket motors ($\sim 10^{-3}$), the acoustic boundary layer may not be assumed to be thin compared to the chamber radius. This invalidates the boundary-layer approach for many cases of interest. However, for the case discussed in the present work, it can be shown that the boundary-layer approximations are valid, due mainly to the high frequencies achieved in the experimental setup. Secondly, Fig. 3 clearly indicates that injection results in increased chamber stability. This latter point resembles the flow turning effect. However, it remains to be evaluated how good an estimation the flow turning is. For further comparison, the damping resulting from the admittance of the boundary layer

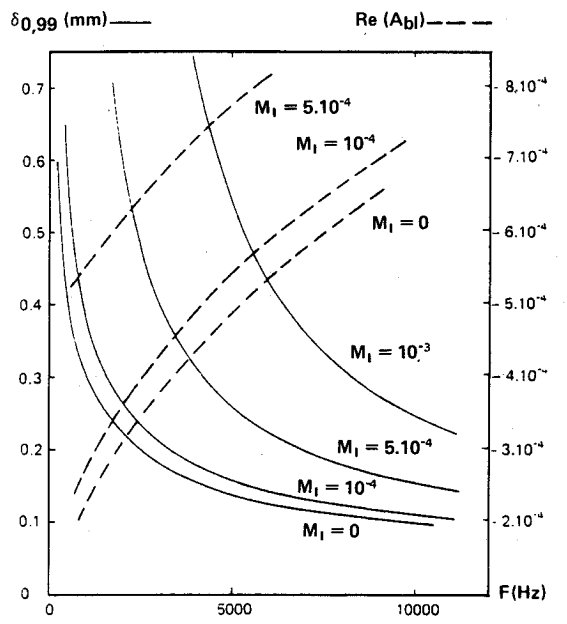

Fig. 3 Boundary-layer thickness at 99% and boundary-layer admittance as functions of F and $\bar{M}_I$; $a_0 = 1000$ m/s; $\mu_0 = 9.10^{-5}$ kg/m/s; $\rho_0 = 6$ kg/m^3.

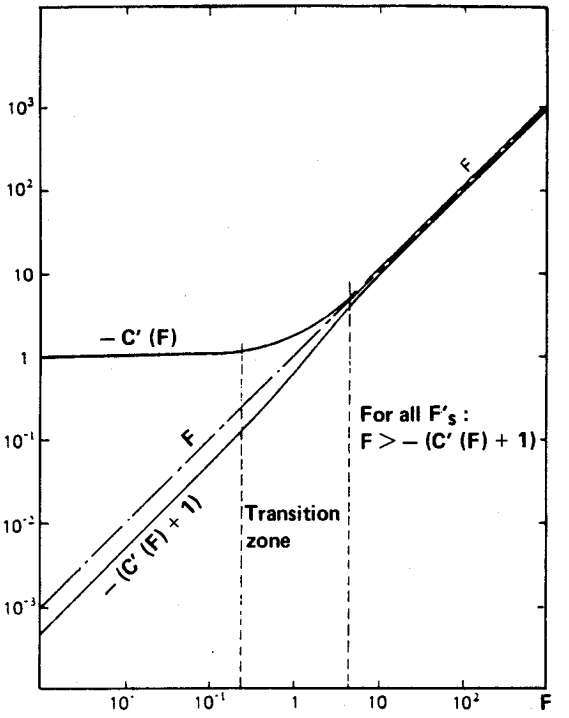

Fig. 4 Dimensionless parameter c' as a function of $F = \bar{M}_I\sqrt{(R_e)_a}$.

can be expressed as

$$\alpha_{BL} = \frac{-a_0}{2E_N^2}\int_{S_b} Re(A_{BL})\hat{p}_N^2 ds$$

C. Comparison of the Two Theories

From the formula giving α_{FT} (Sec. IIA), it can be seen that α_{FT} is proportional to $\bar{M}_I$ so that it vanishes for vanishing $\bar{M}_I$. However, α_{BL}, as derived in Sec. IIB, has a nonzero limit for vanishing $\bar{M}_I$. Incidentally, this limit corresponds to the damping from pure acoustic boundary layers without injection, $(\alpha_{BL})_0$.[8,10] It thus appears that two distinct actions are contained in α_{BL}: one related to pure acoustic boundary layers, which is of order $1/\sqrt{(R_e)_a}$, and one related to the interaction of the injected flow with acoustic motions, which is of order $\bar{M}_I$. For F larger than unity [i.e., $\bar{M}_I > 1/\sqrt{(Re)a}$], both actions (i.e., α_{BL}) are of the order $\bar{M}_I$, at least. Hence, α_{BL} is compatible with the order of the acoustic balance developments ($\bar{M}_I$). However, for $F<1$, terms of order $1/\sqrt{(Re)a}$ become preponderant over terms of order $\bar{M}_I$ and thus cannot be included in classical stability analyses. Nevertheless, if one wants to compare α_{BL} to α_{FT} over the whole range of F (i.e., $\bar{M}_I$), one has to isolate the action of the blowing in α_{BL}. The easiest way of doing this is to let $\Delta\alpha_{BL} = \alpha_{BL} - (\alpha_{BL})_0$. This is readily translated in terms of admittances as

$$\Delta A_{BL} = A_{BL} - (A_{BL})^{\bar{M}_I=0}$$

From Eq. (12) it is easily found that

$$Re(A_{BL}) = c'/\sqrt{(R_e)_a} \text{ with } c' = -2b'/(a'^2 + b'^2)$$

$$Re(\Delta A_{BL}) = (c'+1)/\sqrt{(R_e)_a}$$

Figure 4 gives the variations of c' and $c'+1$ with F. It is found that

$$F \ll 1, \quad Re(A_{BL}) = 1/\sqrt{(R_e)a} - \bar{M}_I/2, \quad Re(\Delta A_{BL}) = -\bar{M}_I/2$$

$$F \gg 1, \quad Re(A_{BL}) = Re(\Delta A_{BL}) = -\bar{M}_I$$

Now, consider a cylindrical grain geometry with a cylindrical axial perforation (Fig. 1) oscillating on one of its longitudinal modes. It is readily found that

$$k_N^2\int_{S_b} (\hat{p}_N)^2 ds = \int_{S_b} (d\hat{p}_N/dx)^2 ds \qquad (13)$$

so that

$$\alpha_{FT} = \frac{a_0}{2E_N^2}\int_{S_b} (\hat{p}_N)^2 \bar{M}_I ds$$

From Fig. 4, it is then found that $\alpha_{FT} > \Delta\alpha_{BL}$ for all F. This implies that the flow turning will always overestimate the damping due to the blowing effect as was already mentioned in the concluding remarks of Sec. IIA.

For practical application, $F \gg 1$, so that $\Delta\alpha_{BL} \simeq \alpha_{BL}$ and, for the remainder of the present work, it is possible to consider the complete effect of α_{BL}. For cylindrical grain geometries and for $F \gg 1$, one verifies that $\alpha_{BL} \simeq \alpha_{FT}$. However, for more complex grain geometries, Eq. (13) no longer holds true, and thus α_{FT} will depart from α_{BL}, mainly due to the structure of the acoustic field. This latter result will be the basis of the experimental work described in the remainder of this paper.

III. Experimental Analysis

A. Experimental Apparatus

The experimental apparatus used in this work is described in detail in Ref. 7 and is currently in use at the ONERA Palaiseau Research Center to determine pressure-coupled response functions of composite propellants at high frequencies (6000-10,000 Hz). A schematic diagram of the apparatus is given in Fig. 5a; Fig. 5b shows the data acquisition scheme. Pressure oscillations at the chamber's first longitudinal mode frequency are generated by means of an intermittent modulation of the exhaust nozzle throat (three-tooth modulating wheel). Figure 6 shows an example of triggered oscillations. The time needed by the modulating wheel to make one revolution is usually sufficient for the oscillations to damp out, so

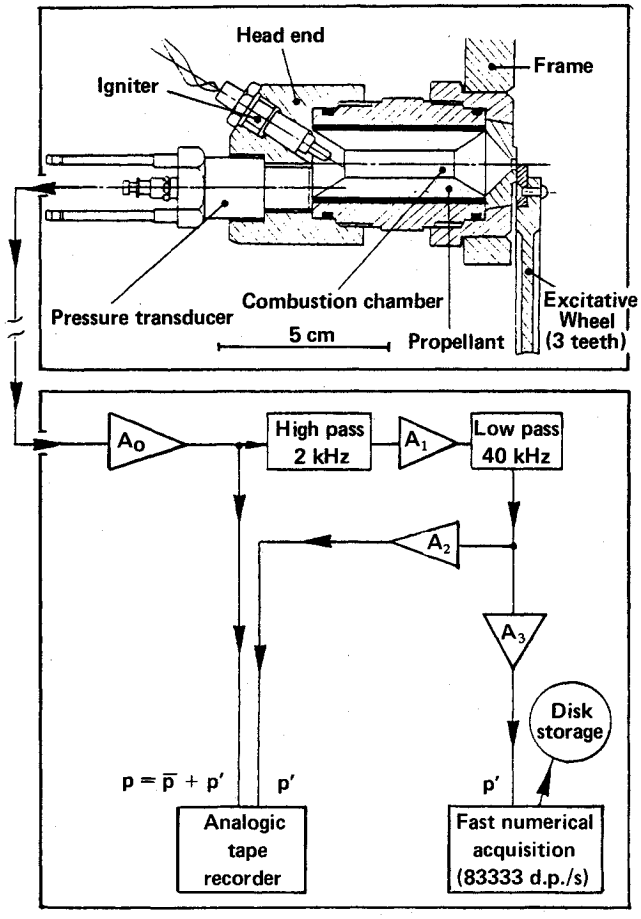

Fig. 5 Experimental apparatus and data acquisition scheme.

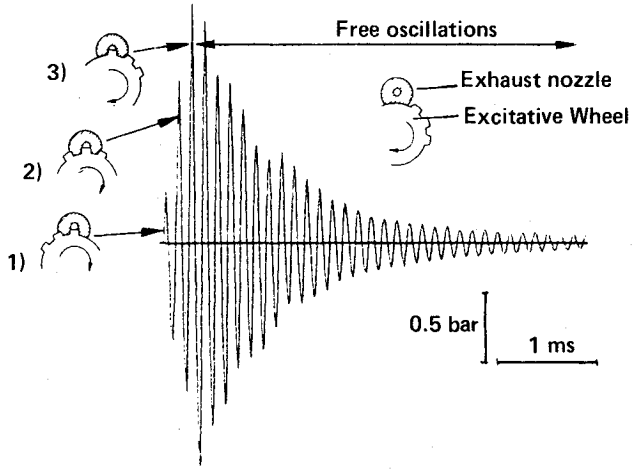

Fig. 6 Example of triggered oscillations.

that the chamber is re-excited from the steady state. Typically, 30-50 successive excitations can be produced during one firing lasting a few tenths of a second. Variations of the mean chamber pressure and of the first longitudinal mode frequency during a firing depend mainly on the grain geometry. This apparatus turned out to be particularly inexpensive to run, since entire portions of response function curves are covered with one firing, that is for high frequencies, 16-20 g of propellant.

The data processing is done in two steps: first, each set of oscillations is analyzed to derive the (f,α) pairs. Then (f,α),

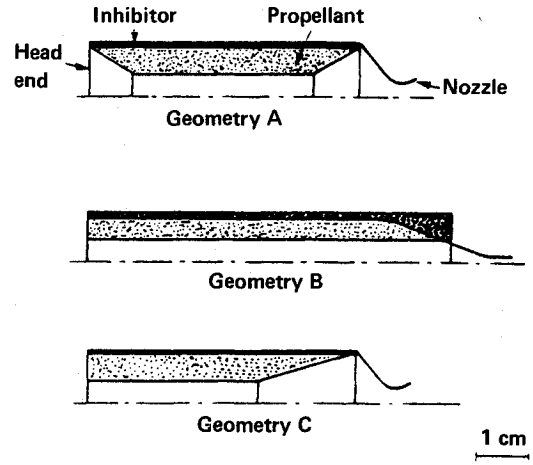

Fig. 7 The three grain geometries.

together with the instantaneous mean chamber pressure and grain geometry, are used as input to an inverse one-dimensional acoustic balance analysis to derive R_c according to Ref. 7. The following improvements have been made with respect to the version presented in Ref. 7:

1) Fast numerical data recording (83333 data points/s) of the unsteady pressure component.

2) Automatic numerical computation of the (f,α) pairs from disk storage, with numerical filtering capabilities. The frequency is derived from the zero crossings of p', and the damping coefficient is deduced from the logarithmic decrement of the extrema of p'. This proved to be the most efficient method in terms of computer time and accuracy (f and α are determined within 1% relative error).

3) Increased acoustic quality of the head end of the small rocket motor by means of an aft and external hot-gas igniter. The head end is thus freed of any ignition device and exhibits a smooth rigid surface, ensuring good pressure wave reflections.

These improvements have greatly simplified and accelerated the data processing.

B. One-Dimensional Stability Analyses

Classical acoustical balance analyses can be inverted to express the propellant response function as a function of the measured complex wave number, $k=\omega/a_0+i\alpha/a_0$ and other contributions.

Flow Turning Analysis

Performing a usual one-dimensional analysis, Ref. 7 arrives at the following formula for $R_e(R_c)$:

$$Re(R_c)=\frac{\gamma-1}{\gamma}+\left(\frac{1+\gamma R_e(V_L)}{\gamma I_2}\right)\tilde{\phi}_{0L}^2$$

$$+\frac{I_3}{\gamma I_2}-\frac{2\alpha L}{a_0\tilde{M}_L}\frac{I_1}{\gamma I_2} \qquad (14)$$

where

$$I_1=\int_0^1 R^2\tilde{\phi}_0^2 dZ$$

$$I_2=\int_0^1 \frac{d(M_1R^2)}{dZ}\tilde{\phi}_0^2 dZ$$

$$I_3=\int_0^1 \frac{d(M_1R^2)}{dZ}\left(\frac{1}{\Omega_0}\frac{d\tilde{\phi}_0}{dZ}\right)^2 dZ$$

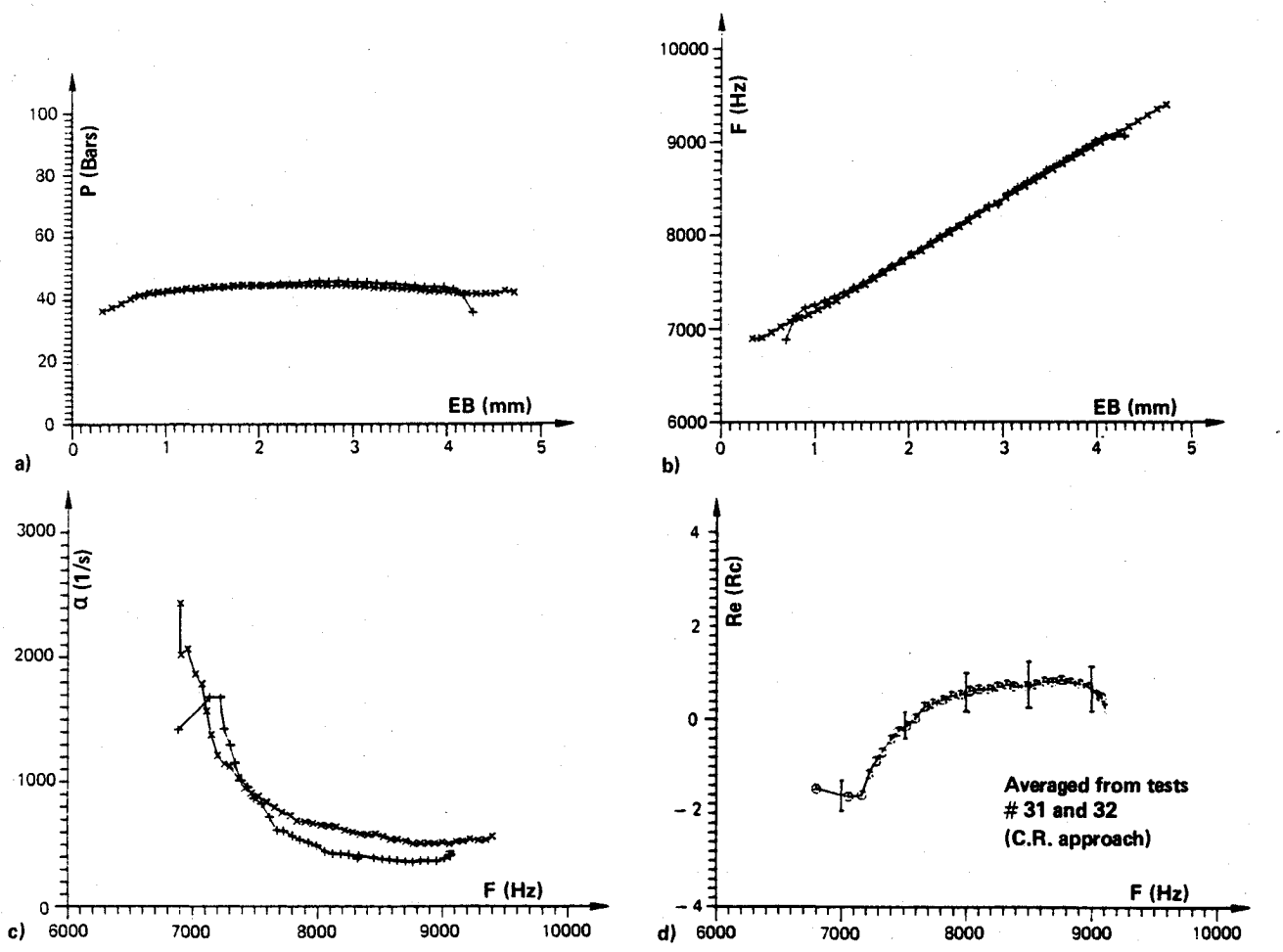

Fig. 8 Experimental results from two firings with geometry A; test numbers 31/83 and 32/83, propellant II.

$Z = x/L$; $R = R(Z)/R_2$; $M_1 = \bar{M}(Z)/\bar{M}_L$

$\Omega_0 = \omega_0 L/a_0$; $\tilde{\phi}_0 = \hat{p}_N/\hat{p}_N(0)$

$V_L = (u'_N/\bar{u})/(p'_N/\bar{p})_L$ (nozzle dimensionless admittance)

R_2 = propellant grain external radius

$\bar{M}_L$ = Mach number at the nozzle entrance plane

It should be noted that the third term of the right-hand side of Eq. (14) corresponds to the flow turning term as it naturally appears in usual one-dimensional analyses.

Admittance Correction Analysis

Let A_b be the burning propellant admittance. When the burning surface is submitted to grazing acoustic waves, an acoustic boundary layer develops. For linear analysis, this simply adds an extra admittance A_{BL} to A_b, so that the apparent propellant admittance at the boundary-layer edge is

$$A_b^* = A_b + A_{\mathrm{BL}} \tag{15}$$

A_b can always be expressed as a response function R_c, $R_c = (v'_c/\bar{v}_c)/(p'/\bar{p}) + (T'/\bar{T})/(p/\bar{p})$. Continuity of mass at the propellant edge, together with the perfect gas equation, leads to $R_c = (v'/\bar{v})/(p'/\bar{p}) + 1$. The following relationship between R_c and A_b is finally obtained:

$$R_c = A_b/\gamma\bar{M}_I + 1 \tag{16}$$

Equation (16) is quite general and allows one to express Eq. (15) in terms of response functions:

$$(R_c)^* = R_c + A_{\mathrm{BL}}/\gamma\bar{M}_I \tag{17}$$

The last term of Eq. (17) can be viewed as a correction to the propellant response function due to the developing of acoustic boundary layers above the burning surface. Then, Eq. (14) yields

$$R_e(R_c) = \frac{\gamma-1}{\gamma} + \left(\frac{1+\gamma Re(V_L)}{\gamma I_2}\right)\tilde{\phi}_{0L}^2 - \frac{Re(A_{\mathrm{BL}})}{\gamma\bar{M}_I} - \frac{2\alpha L}{a_0\bar{M}_L}\frac{I_1}{\gamma I_2} \tag{18}$$

One should notice that the flow turning term of Eq. (14) is replaced by the correction of response function $-Re(A_{\mathrm{BL}})/\gamma\bar{M}_I$. This term tends to $1/\gamma$ for large F.

C. Experimental Results

Experimental Conditions

In order to illuminate the difference between the flow turning (FT) and the admittance correction (hereafter named CR, for correction of response) approaches, three grain geometries have been devised and are displayed in Fig. 7. During a firing, geometry A provides an almost constant mean chamber pressure while the frequency roughly increases linearly with time. This is the standard grain geometry for the experimental

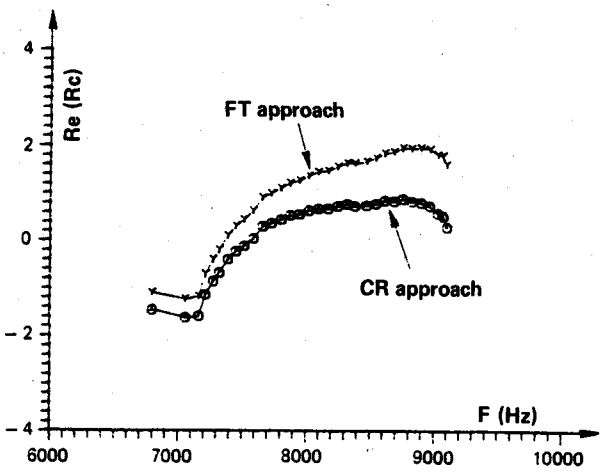

Fig. 9 Difference between the CR and FT theoretical approaches; geometry A, propellant II, test no. 31-32.

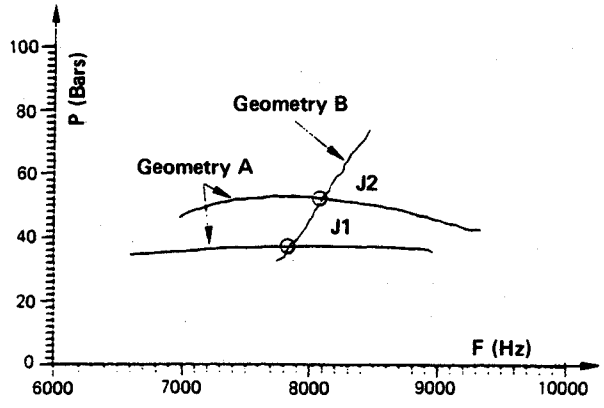

Fig. 10 *p-f* histories for propellant I.

apparatus.[7] Geometry B is purely cylindrical and thus provides an almost constant frequency while the mean chamber pressure is monotonously increasing during the firing. Geometry C is an intermediate one.

It has already been demonstrated in Sec. IIC that both approaches give similar results for geometry B. For geometry A, it can be shown that the two approaches differ greatly, owing to the combustion concentrating at acoustic velocity antinodes during the firing. Geometry C exhibits an intermediate behavior.

Figures 8a-d show examples of experimental results as measured from two firing tests performed with A geometry propellant grain. Measured standard deviations are found to be: 1 bar (3%) for $\bar{p}$, 50 Hz (1%) for f, and 90 s^{-1} ($\sim$9%) for α, resulting in an absolute error in $Re(R_c)$ close to ± 0.40.

From Figs. 8a-d, it is clear that the main source of experimental error lies in the determination of α and, indeed, it is found that $R_e(R_c)$ is very sensitive to α. Before comparing the two theoretical approaches on experimental grounds, one has to make sure that the experimental errors do not exceed the differences resulting from the theoretical treatments. An idea of the sensitivity of $Re(R_c)$ to α can be obtained by differentiating either Eq. (14) or Eq. (18) with respect to α:

$$\sigma = \partial[Re(Rc)]/\partial\alpha = -(2L/a_0\bar{M}_L)/(I_1/\gamma I_2)$$

During a firing, I_1 and I_2 (thus σ) vary according to the grain geometry. Variations of I_1 and I_2 are shown for geometry A in Fig. 23 of Ref. 7. For the present work, Table 1 only indicates the range of variation of I_1/I_2 and σ for the three geometries. The absolute error in $R_e(R_c)$ due to experimental error $\Delta\alpha$ is roughly $\Delta R_c = \sigma\Delta\alpha$.

Figure 9 shows that for geometry A the difference between the two theories in terms of $R_e(R_c)$ varies roughly from 0.40 to 1.33. For geometry B the difference is almost zero, owing to the high values of the parameter F ($F \sim 5$), and for geometry C it varies from 0.10 to 0.40. Considering geometry A (which is the most sensitive to the theoretical treatment), and taking $\Delta\alpha \simeq 200\ s^{-1}$ from Fig. 8c, one finds that the experimental er-

Table 1 Theoretical values of $\Delta R_c/\Delta\alpha$, $a_0 = 1050$ m/s, $\gamma = 1.216$

	Geometry A	Geometry B	Geometry C
L,m	0.050	0.063	0.050
$\bar{M}_L$	0.015	0.050→0.020	0.015
I_1/I_2	0.37→2.02	1	0.34→1.18
$\sigma = \lvert \Delta R_c/\Delta\alpha \rvert$, s	0.0019→0.0105	0.0020→0.0049	0.0018→0.0062

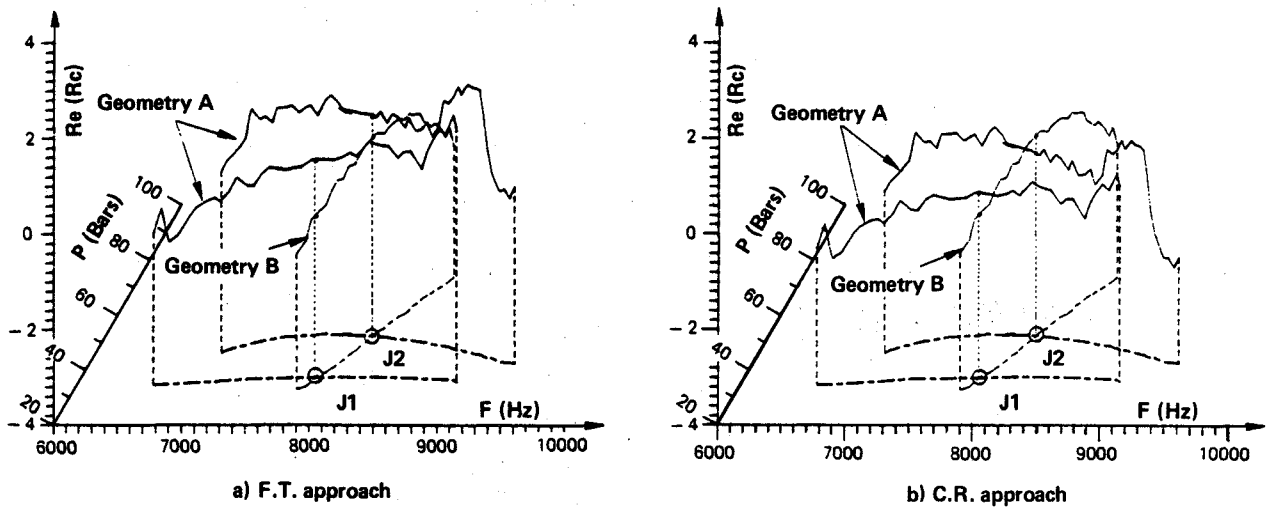

Fig. 11 Response function curves by means of both approaches —propellant I.

ror in $R_e(R_c)$ will be reasonably less than the theoretical difference, except at the very end of the firing.

Then the A, B, and C geometries were test-fired with two different composite propellants, CTPB+AP (82%). Each time, intersections in the pressure-frequency plane have been looked for, with the argument that the proper approach should yield the same values for $R_e(R_c)$, irrespective of the particular grain geometry, provided the same frequency and mean chamber pressure are achieved in the chamber.

Results for Propellant I

Only geometry A and B have been tested with propellant I. As far as possible, the results presented are averaged over several firings performed under similar conditions. Figure 10 shows the $\bar{p}$-f histories obtained; it can be seen that sharp intersections are achieved. Response function curves derived for both geometries and by means of both approaches are presented in Figs. 11a and 11b. From these figures, it is clear that the CR approach provides the best agreement, while the FT approach leads to an overestimated $Re(R_c)$ in the case of geometry A, due to its $(d\hat{p}_N/dx)$ dependence. Precise values at intersection points are given in Table 2.

Results for Propellant II

This propellant is the one already mentioned in Ref. 7, and some of the results presented hereafter are taken from this reference. For the present work, propellant II has been tested on all three grain geometries. However, practical difficulties related to propellant aging arose and prevented a satisfactory check of the results presented for geometry B. Moreover, geometry C systematically exhibited lower values of $Re(R_c)$ with no explanation being found for this behavior. Under such conditions, no definitive conclusions should be drawn from the following results. However, they are believed to give an indication of the tendencies and are thus worth mentioning.

Six independent $Re(R_c)$ curves have been derived from several experiments and led to seven intersection points in the $(f$-$\bar{p})$ plane (Fig. 12). These points decompose into four B-A intersections (J_1 to J_4), one B-C intersection (J_5), and two C-A intersections (J_6 and J_7). The analogs of Figs. 11 are not given, owing to the complexity resulting from the great number of curves. The results are summarized in Table 3. Despite a more important scattering due to the above-mentioned difficulties, it is clear that the results of Table 3 confirm that the CR approach yields better agreement than the FT approach.

Discussion

From the nine intersection points of Tables 2 and 3, it is found that the mean of the absolute values of the deviations in $R_e(R_c)$ due to differing grain geometries turns out to be 1.47 (s.d. 0.68) for the FT approach and 0.83 (s.d. 0.47) for the CR approach. Moreover, if the comparison is limited to the B-A intersections (6 points), which seem sharper, the mean values of the signed deviations are, respectively, −1.38 (s.d. 0.54)

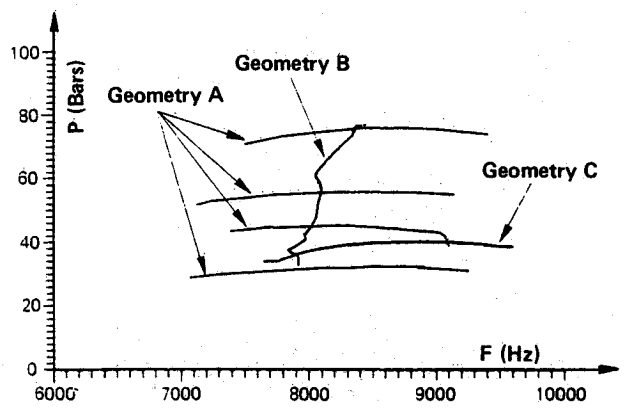

Fig. 12 p-f histories for propellant II.

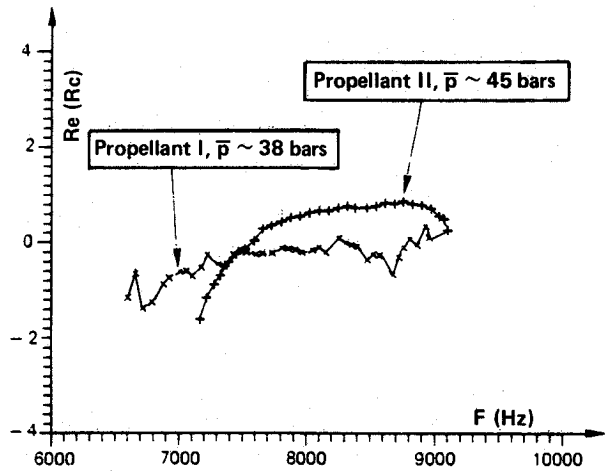

Fig. 13 Example of response function curves—propellants I and II—CR approach, geometry A.

Table 2 Values of $R_e(R_c)$—propellant I

	$Re(R_c)_{FT}$		$Re(R_c)_{CR}$		$\Delta[Re(R_c)]$	
Intersection points	B	A	B	A	FT	CR
J_1: (7800 Hz-37 b)	−0.60	+0.60	−0.60	−0.13	−1.20	−0.47
J_2: (8100 Hz-52 b)	+0.13	+0.67	+0.13	−0.17	−0.54	+0.30

Table 3 Values of $Re(R_c)$—propellant II

	Geometry		$Re(R_c)_{FT}$		$Re(R_c)_{CR}$		$Re(R_c)$	
Intersection points	1	2	Geometry 1	Geometry 2	Geometry 1	Geometry 2	FT	CR
J_1 (7900 Hz-32 b)	B	A	−0.10	+1.15	−0.10	+0.27	−1.25	−0.37
J_2 (8025 Hz-46 b)	B	A	−0.07	+1.33	−0.07	+0.60	−1.40	−0.67
J_3 (8090 Hz-56 b)	B	A	+0.90	+2.60	+0.90	+1.80	−1.70	−0.90
J_4 (8350 Hz-76 b)	B	A	−1.30	+0.87	−1.30	−0.07	−2.17	−1.23
J_5 (7900 Hz-35 b)	B	C	−0.30	−0.90	−0.30	−0.97	+0.60	+0.67
J_6 (7650 Hz-32 b)	C	A	−0.97	+0.73	−1.07	0.00	−1.70	−1.07
J_7 (9100 Hz-40 b)	C	A	−1.00	+1.65	−1.37	+0.40	−2.65	−1.77

and -0.56 (s.d. 0.52). In both cases, deviations related to the FT approach appear to lie beyond experimental uncertainties and to be linked to overestimated propellant response when geometry A is employed. On the other hand, the CR approach appears to be less sensitive to the grain geometry. Despite the difficulties related to the aging of propellant II, experimental results seem to validate the CR approach against the FT one.

Finally, examples of response curves derived by means of the CR method are given for each propellant (Fig. 13). Propellant II exhibits a stronger R_c in the 8,000-9,000-Hz frequency range while a rather flat behavior is found for propellant I, which exhibits an almost zero response.

IV. Conclusions

The experimental apparatus implemented at ONERA to determine pressure-coupled solid propellant response functions at high frequencies has been utilized to compare two theoretical models predicting viscosity-related acoustic losses. The apparatus turned out to be very inexpensive to run, and values of the response functions have been derived for two composite propellants over wide ranges of pressure and frequency. Despite practical difficulties related to the aging of one of the two propellants used, final results tend to favor the viscous flow model over the flow turning model. This should contribute to a better prediction of solid propellant rocket motor stability domains, especially when complex grain geometries are involved.

Acknowledgments

Part of this work has been supported by "Direction des Recherches et Etudes Techniques, Délégation Générale à l'Armement," France, and by "Société Nationale des Poudres et Explosifs," France. We also wish to express special thanks to F. Cauty and C. Caugant of ONERA for their support in the experimental and numerical tasks.

References

[1]Hart, R. W. and McClure, F. T., "Theory of Acoustic Instability in Solid-Propellant Rocket Combustion," 10th International Symposium on Combustion, The Combustion Institute, Pittsburgh, PA, 1965, pp. 1047-1065.

[2]Culick, F. E. C., "Acoustic Oscillations in Solid Propellant Rocket Chambers," *Astronautica Acta*, Vol. 12, No. 2, 1966, pp. 113-125.

[3]Culick, F. E. C., "The Stability of One-Dimensional Motions in a Rocket Motor," *Combustion Science and Technology*, Vol. 7, 1973, pp. 165-175.

[4]Culick, F. E. C., "Stability of Three-Dimensional Motions in a Combustion Chamber," *Combustion Science and Technology*, Vol. 10, 1975, pp. 109-124.

[5]Flandro, G. A., "Solid Propellant Acoustic Admittance Corrections," *Journal of Sound and Vibration*, Vol. 36, No. 3, 1974, pp. 297-312.

[6]Van Moorhem, W. K., "Flow Turning in Solid Propellant Rocket Combustion Stability Analyses," *AIAA Journal*, Vol. 20, Oct. 1982, pp. 1420-1425.

[7]Kuentzmann, P. and Laverdant, A., "Détermination Expérimentale de la Réponse d'un Propergol Solide aux Oscillations de Pression de Haute Fréquence," *La Recherche Aérospatiale*, No. 1, 1984, pp. 39-55 (English translation available).

[8]Vuillot, F. and Avalon, G., "Instabilités de Combustion des Propulseurs à Propergols Solides," ONERA—RTS 41/3725 E, April 1984.

[9]Kuentzmann, P. and Nadaud, L., "Réponse des Propergols Solides aux Oscillations de Pression et de Vitesse," *Combustion Science and Technology*, Vol. 11, 1975, pp. 119-139.

[10]Morse, P. M. and Ingard, K. U., "Theoretical Acoustics," McGraw-Hill Book Co., New York.